Bifurcation Analysis of a Rotor Supported by Five-Pad Tilting Pad Journal Bearings Using Numerical Continuation

Sitae Kim
Department of Mechanical Engineering,
Texas A&M University,
College Station, TX 77840
e-mail: sitaekim@tamu.edu

Alan B. Palazzolo[1]
Professor
Fellow ASME
Department of Mechanical Engineering,
Texas A&M University,
College Station, TX 77840
e-mail: a-palazzolo@tamu.edu

This paper presents analytical bifurcations analysis of a "Jeffcott" type rigid rotor supported by five-pad tilting pad journal bearings (TPJBs). Numerical techniques such as nonautonomous shooting/arc-length continuation, Floquet theory, and Lyapunov exponents are employed along with direct numerical integration (NI) to analyze nonlinear characteristics of the TPJB-rotor system. A rocker pivot type five-pad TPJB is modeled with finite elements to evaluate the fluid pressure distribution on the pads, and the integrated fluid reaction force and moment are utilized to determine coexistent periodic solutions and bifurcations scenarios. The numerical shooting/continuation algorithms demand significant computational workload when applied to a rotor supported by a finite element bearing model. This bearing model may be significantly more accurate than the simplified infinitely short-/long-bearing approximations. Consequently, the use of efficient computation techniques such as deflation and parallel computing methods is applied to reduce the execution time. Loci of bifurcations of the TPJB-rigid rotor are determined with extensive numerical simulations with respect to both rotor spin speed and unbalance force magnitude. The results show that heavily loaded bearings and/or high unbalance force may induce consecutive transference of response in forms of synchronous to subsynchronous, quasi-periodic responses, and chaotic motions. It is revealed that the coexistent responses and their solution manifolds are obtainable and stretch out with selections of pad preload, pivot offset, and lubricant viscosity so that the periodic doubling bifurcations, saddle node bifurcations, and corresponding local stability are reliably determined by searching parameter sets. In case the system undergoes an aperiodic state, the rate of divergence/convergence of the attractor is examined quantitatively by using the maximum Lyapunov exponent (MLE). [DOI: 10.1115/1.4037699]

1 Introduction

Modern rotating machinery, such as gas/steam turbines, generators, compressors, gearboxes, and pumps, experience higher performance and efficiency as the number of stages and speed increase. However, this change tends to increase the propensity of the machines for rotordynamic instability. Symptoms of nonlinear vibration have been observed in industrial, typically, when the bearings are operating at high eccentricity due to misalignment, gear, hydraulic, or gravity induced static loads. This may also occur when large levels of mass imbalance develop due to erosion, accumulation of deposits, partial blade loss, etc. This anomalous operation occurs more often in process critical machines that typically operate 24/7 for 5 yr or more continuous, between scheduled downtimes for maintenance and replacement.

Tilting pad journal bearings (TPJBs) have been selected in such machines due to their stabilizing effects on the rotor systems; the tilting motions of pads greatly suppress the cross-coupled stiffness coefficients and thus enhance rotor stability. Nonetheless, a survey of the literature reveals that TPJBs do not always perform successfully.

Pagano et al. [1] and Brancati et al. [2] used numerical integration (NI) to determine that an unbalanced rotor supported by TPJBs may experience subsynchronous motions with one-half or one-quarter components under certain operating conditions. Abu-Mahfouz and Adam [3] used numerical integration to determine that an unbalanced rotor supported by three-pad TPJBs may experience quasi-periodic and chaotic responses. Cao et al. [4] used numerical integration to determine that a complex flexible rotor, eight-stage centrifugal compressor, supported by TPJBs, exhibited strong nonlinear behaviors such as sub- and supersynchronous responses. Gadangi et al. [5,6] indicated that large, multiharmonic orbital motions occur in TPJB supported machines with high levels of unbalance and are affected by pad deformations and fluid thermal effects. Suh and Palazzolo [7] investigated thermally induced synchronous instability, i.e., Morton effect, in TPJBs using three-dimensional structural finite elements models for the shaft and pads, a variable viscosity Reynolds equation, and the three-dimensional energy equation. So far, a considerable amount of numerical studies has been conducted to predict instability and nonlinear dynamic characteristics of TPJB-rotor systems, most of them rely on transient numerical integrations.

Steady-state, nonlinear dynamics, search-based approaches such as harmonic balance, trigonometric collocation, and shooting/continuation have seldom been used for the analyzing the nonlinear response of TPJB supported rotors. These approaches use numerical integration to iteratively determine initial states of all coexistent periodic responses, their local stability, and bifurcation onsets. However, the use of this approach requires an extensive amount of computations to evaluate Jacobian matrices iteratively in the solution procedure. This limited previous studies to considering Jeffcott type rotor models supported on simple geometry bearings [8–14], for instance, floating ring bearings, squeeze film dampers, and plain journal bearings, which are suitable for providing fluid film forces obtained from infinitely short-/long-bearing theories.

In the present paper, an improved nonautonomous shooting/arc-length continuation method is employed to analyze nonlinear behaviors of rotors supported on TPJBs. An objective of this research is to identify bifurcations and coexistent responses including both stable and unstable solutions. In addition, effects

[1]Corresponding author.

Contributed by the Tribology Division of ASME for publication in the Journal of Tribology. Manuscript received September 28, 2016; final manuscript received August 8, 2017; published online September 29, 2017. Assoc. Editor: Joichi Sugimura.

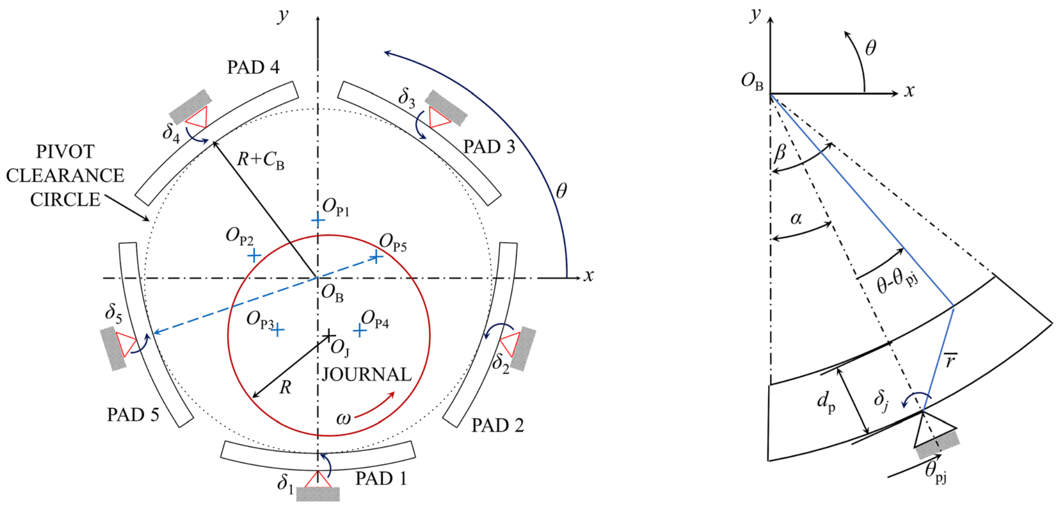

Fig. 1 Five-pad TPJB (load on pad) diagram and the respective coordinates in *x–y* plane

of pad preload, pivot offset, and lubricant viscosity on rotordynamic bifurcations are investigated. Due to the geometrical and dynamical complexity of TPJBs, simplified fluid film models have limitation to evaluate fluid film pressure on the pads so that a finite element-based TPJB model with rigid rocker pivots is developed for the bifurcation study. Efficient execution algorithms such as deflation and parallel computing are employed in order to reduce the corresponding computation time.

Original contributions of this research are:

- Development of the nonautonomous shooting and arc-length continuation algorithms for TPJB applications. TPJBs are the most common bearing type in critical, high rpm rotating machinery.
- Numerical identification of bifurcations, multiple (coexisting) responses states, and chaos of a TPJB rotodynamic system.
- Parametric study with the numerical continuation method for analyzing effects of pad preload, pivot offset, and lubricant viscosity to the nonlinear behaviors of TPJBs. These are parameters that are varied by machinery designers to obtain optimal vibration control.

2 Rotor-Bearing Model

2.1 Finite Element Tilting Pad Journal Bearings Model. Figure 1 depicts the middle plane in the axial direction of a TPJB model and its coordinate system. The film thickness distribution for a given pad is dependent on the x and y components of the journal center and on the pad angle δ_j, as given by the formula

$$h(\theta) = C_{Pj} - X\cos(\theta) - Y\sin(\theta) - (C_{Pj} - C_B)\cos(\theta - \theta_{Pj}) - \delta_j R\sin(\theta - \theta_{Pj}) \tag{1}$$

where $h(\theta)$ is film thickness at angular location θ, C_{Pj} is the radial pad clearance of pad j, C_B is the radial bearing clearance, X and Y are x and y components of the journal's displacement relative to bearing center O_B, δ_j is the rotation angle of pad j, R is the journal radius, and θ_{Pj} is value of θ at the pivot of pad j.

The hydrodynamic pressure on the fluid film of each pad, p, can be determined from Reynolds equation for an incompressible and isoviscosity lubricating oil model, as follows:

$$\frac{\partial}{\partial\theta}\left(\frac{h^3}{12\mu}\frac{\partial p}{\partial\theta}\right) + \frac{\partial}{\partial z}\left(\frac{h^3}{12\mu}\frac{\partial p}{\partial z}\right) = \frac{R\omega}{2}\frac{\partial h}{\partial\theta} + \frac{\partial h}{\partial t} \tag{2}$$

where z is the axial direction of the bearing, μ is dynamic viscosity, and ω denotes the rotational speed of journal. The solution of Reynolds equation is obtained using a finite element model, which consists of a three-node simplex, triangular type mesh generated on half of fluid film layer in the axial direction with an assumption of a symmetrical pressure state. Fluid reaction force between a pad and the journal is obtained by integrating the pressure throughout the mesh and multiplying by 2 to account for the other half of the bearing

$$\begin{Bmatrix} F_{xj} \\ F_{yj} \end{Bmatrix} = 2\int_0^{L/2}\int_{\theta_{Bj}}^{\theta_{Ej}} p_j(\theta, y)\begin{Bmatrix} -\cos(\theta) \\ -\sin(\theta) \end{Bmatrix} d\theta dz \tag{3}$$

where θ_{Bj} is the beginning angle of pad j, and θ_{Ej} is the end angle of pad j.

The total, lubricant film force on the journal is

$$\begin{Bmatrix} F_x \\ F_y \end{Bmatrix} = \sum_{j=1}^{N_p}\begin{Bmatrix} F_{xj} \\ F_{yj} \end{Bmatrix} \tag{4}$$

The pressure distribution on pad j induces a moment on the pad about its pivot

$$M_{Pj} = 2\int_0^{L/2}\int_{\theta_{Bj}}^{\theta_{Ej}} p_j(\theta, y)\,\mathbf{r} \times \begin{Bmatrix} \cos(\theta) \\ \sin(\theta) \end{Bmatrix} R d\theta dz \tag{5}$$

where $\mathbf{r}$ is the vector from the pivot contact point on pad j to the location of the differential force on pad j. Figure 2 shows the finite element TPJB model used in this study and an example of pressure distributions on the pads. Note that the Reynolds equation used for determining the lubricant pressure distribution does not model a highly turbulent flow state. This restricts the application of the Reynolds equation to moderate speed ranges, which includes all results presented in this paper.

2.2 Dynamics of a Symmetric Rigid Rotor Supported by Tilting Pad Journal Bearings. A Jeffcott type symmetric rigid rotor supported by five-pad tilting pad journal bearings (TPJB-RGD) is set to as a mechanical model for investigation of nonlinear response and bifurcation behaviors, as can be seen in Fig. 3. The bearing specification, parameter ranges, and pressure boundary conditions are specified in Table 1. Spin speeds and rotor mass are varied in the TPJB-RGD system model for the parametric study.

The equations of motion for the journal and pads can be written as

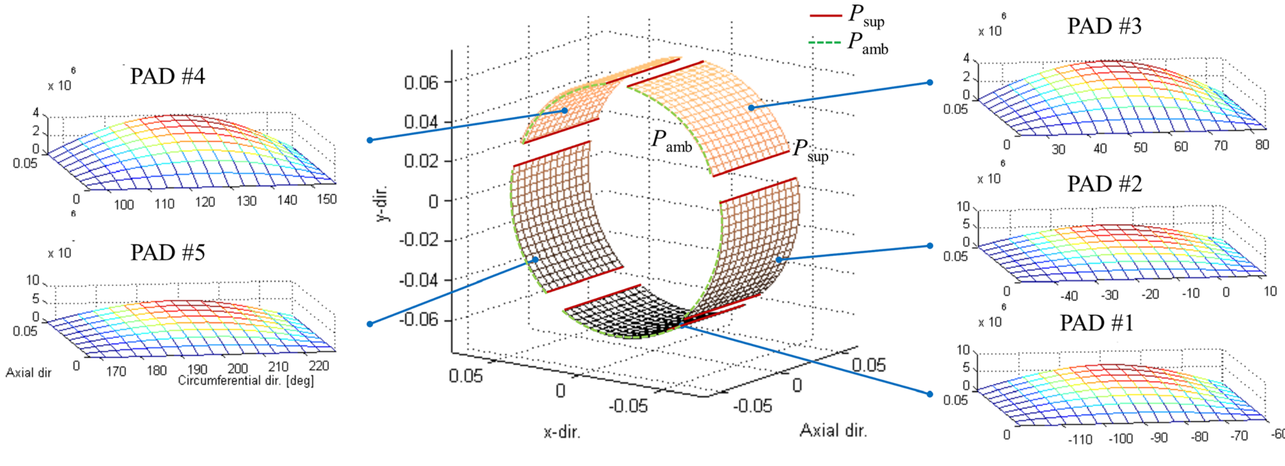

Fig. 2 Finite element TPJB model and typical pressure distributions on pads

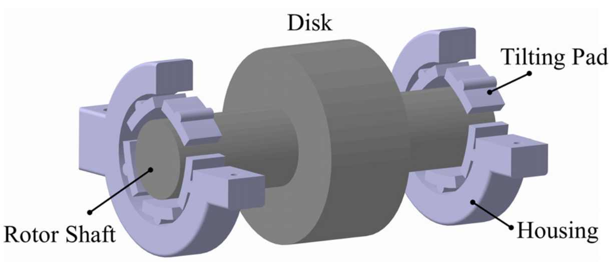

Fig. 3 Symmetric TPJB support—rigid rotor system

$$\begin{aligned} M_J\ddot{x} &= F_x + W_{dx} + W_{sx} \\ M_J\ddot{y} &= F_y + W_{dy} + W_{sy} \\ I_{pj}\ddot{\delta}_{pj} &= M_{pj} \end{aligned} \tag{6}$$

where M_J is the rotor mass, I_p is the pad inertia, W_s and W_d are static and dynamic loads on the bearing, and M_p is the integrated moments on the pad. The static force can be the weight of rotor/disk or side loads, and the dynamic force is usually due to unbalance force, F_{imb}, from imbalance eccentricity, e_{imb}, on the rotor/disk.

3 Method of Solution

3.1 Shooting, Arc-Length Continuation, and Floquet Theory. The unbalance force acts on the rotor at a period equal to the spin period (τ_s). A periodic solution has an orbital equilibrium states satisfying

$$\mathbf{f}(\mathbf{x}_0, \tau_s) = \mathbf{x}_T(\mathbf{x}_0, \tau_s) - \mathbf{x}_0 = 0 \tag{7}$$

where $\mathbf{x}_0$ is the initial condition of the orbital equilibrium states, and $\mathbf{x}_T$ ($\mathbf{x}_0$, τ_s) is the state vector after period τ_s, which should be identical and satisfy Eq. (6). Solutions of Eq. (7) are obtained as follows.

Let $\mathbf{x}_0^i$ be a first guess of a root of the function $\mathbf{f}$ in Eq. (7), and expand $\mathbf{f}$ in a two-term Taylor series

$$\mathbf{f}\left(\mathbf{x}_o^i\right) + \frac{d\mathbf{f}(\mathbf{x}_o)}{d\mathbf{x}_o}\bigg|^i d\mathbf{x}_o^i = 0 \tag{8}$$

where $d\mathbf{x}_0^i = \mathbf{x}_0^{i+1} - \mathbf{x}_0^i$. Then, substitute Eq. (8) into Eq. (7) to yield

$$\mathbf{x}_0^i - \mathbf{x}_T(\mathbf{x}_0^i) + [\mathbf{J}_x^i - \mathbf{I}]\{\mathbf{x}_0^{i+1} - \mathbf{x}_0^i\} = 0 \tag{9}$$

where $\mathbf{J}_x^i = ((d\mathbf{x}_T(\mathbf{x}_o, \tau_s))/d\mathbf{x}_o^i) = [(\partial\mathbf{x}_T/\partial x_o^1) \; \ldots \; (\partial\mathbf{x}_T/\partial x_o^n)]^i$ is a Jacobian matrix, and $\mathbf{I}$ is an identity matrix.

Newton's method iteratively provides periodic states, which satisfy Eq. (7), and can be expressed as

$$\mathbf{x}_0^{i+1} = \mathbf{x}_0^i + [\mathbf{J}_x^i - \mathbf{I}]^{-1}\{\mathbf{x}_0^i - \mathbf{x}_T(\mathbf{x}_0^i)\} \tag{10}$$

Solutions obtained from the shooting method are located at beginning points of a path-following procedure to track solution manifolds and bifurcations with respect to an operating parameter (η). The arc-length continuation method is adopted for that purpose in this research. In the procedure, an arc-length of the solution curve, s, is utilized as a parameter to predict the periodic solution of the next step of the operating parameter, and Newton's method provides an update such that

$$\begin{Bmatrix} \mathbf{x}_n^{i+1} \\ \eta_n^{i+1} \end{Bmatrix} = \begin{Bmatrix} \mathbf{x}_n^i \\ \eta_n^i \end{Bmatrix} + \begin{bmatrix} \mathbf{J}_x^i & \mathbf{J}_\eta^i \\ \dfrac{\partial {q_n^i}^{\mathrm{T}}}{\partial \mathbf{x}} & \dfrac{\partial q_n^i}{\partial \eta} \end{bmatrix}^{-1} \begin{Bmatrix} -\mathbf{f}\left(\mathbf{x}_n^i, \eta_n^i\right) \\ -q\left(\mathbf{x}_n^i, \eta_n^i, s\right) \end{Bmatrix} \tag{11}$$

where $\mathbf{J}_\eta$ is Jacobian matrix with respect to η, and q is the additional constraint function: $q(\mathbf{x}, \eta, s) = \zeta\|\mathbf{x}_{n+1}^i - \mathbf{x}_n\|_2^2 + (\zeta_{n+1}^i - \zeta_n)^2 - (\Delta s)^2 = 0$.

Table 1 TPJB specifications and parameter ranges

Bearing parameter	Value (unit)	Pad parameter	Value (unit)
Journal diameter (D)	0.1016 (m)	Number of pads (arc-length)	5 (60 deg, load on pad)
Bearing length (L)	0.0508 (m)	Preload (m_p)	1/2, 2/3
Spin speed	1–20 (krpm)	Offset (α/β)	0.5, 0.6
Bearing load (W)	4.9, 9.8, 19.6 (kN)	Bearing clearance (C_b)	81.3 (μm)
Lubricant viscosity (μ)	10.3, 13.8, 27.0 (mPa·s)	Pad clearance (C_p)	162.5, 243.8 (μm)
Amounts of imbalance on disk (e_{imb})	0.05–0.3C_b	Pad thickness	0.02 (m)
Lubricant supply pressure (P_{sup})	10^5 (Pa)	Lubricant ambient pressure (P_{amb})	0 (Pa)

The convergence limits for the shooting and continuation are set as $\|\mathbf{x}_0^{i+1}-\mathbf{x}_0^i\|/\|\mathbf{x}_0^i\|=10^{-7}$.

The local stability of the periodic solutions from the shooting/continuation can be determined by Floquet theory. In the procedure, the eigenvalues of monodromy matrix are used to predict local stability and bifurcation scenarios. Numerical details of the shooting, arc-length continuation, and Floquet theory are well described in Ref. [15].

3.2 Deflation Algorithm and Parallel Computing. Prior work that utilized the shooting/continuation methods for rotordynamics relied on infinitely short-/long-bearing approximations that correspond to relatively simple geometry bearing models such as plain journal or floating bushing bearings. In contrast, the present study is conducted using finite length, preloaded, multipad tilting pads constrained by pivots. The increase computation load resulting from the complexity of the tilting pads is reduced by using deflation and parallel computing strategies.

A deflation algorithm includes a mathematical modification of the original system in order to determine additional, not yet found, solutions of multiple root nonlinear equations [16,17]. The method is based on the practice that once a root has been determined, the original system is modified using all previously found solutions, so that these are no longer roots of the new system. The deflated function $\hat{\mathbf{f}}(\mathbf{x}_o,\tau_o)$ employs a denominator function h, which is a series product of relative Euclidean norms of the previously found solution vectors as

$$\hat{\mathbf{f}}(\mathbf{x}_o,\tau_o)=\frac{\mathbf{f}(\mathbf{x}_o,\tau_o)}{h(\mathbf{x}_o)},\quad \text{where}\quad h(\mathbf{x}_0)=\prod_{j=1}^{p}\|\mathbf{x}_0^i-\mathbf{x}_{0j}\| \tag{12}$$

The shooting method then searches for further solutions with the modified function. The corresponding formulations of Eqs. (7)–(10) including the modified function provide the nonautonomous shooting with deflation algorithm

$$\mathbf{x}_0^{i+1}=\mathbf{x}_0^i+\left[-h(\mathbf{x}_0)^{-2}\frac{\partial h}{\partial \mathbf{x}_0}(\mathbf{x}_T(\mathbf{x}_0)-\mathbf{x}_0)+h^{-1}(\mathbf{x}_0)(\mathbf{J}_x-\mathbf{I})\right]^{-1}\times\frac{\mathbf{x}_0^i-\mathbf{x}_T(\mathbf{x}_0^i)}{h(\mathbf{x}_0^i)} \tag{13}$$

A second strategy for faster execution is the adoption of parallel computing methods. The parallelized numerical routines for obtaining Jacobian matrices in the shooting and continuation algorithms can significantly reduce computation time such that the boundary value problems with perturbed initial conditions are isolated from each other and solved simultaneously. Thus, multiple numerical time integrations, here fourth-order Runge–Kutta, are executed in parallel. The desired number of carriers, i.e., multiprocessors, depends on the system states dimension and the shooting/continuation parameters. For instance, this work utilizes 15 cores for shooting and 16 cores for continuation.

Figure 4 depicts the flow chart of the improved shooting algorithm for rotordynamic system. The highlighted sections of the chart designate the deflation and parallel computing techniques.

The efficiency of deflation and parallel computing is examined by solving a nonlinear dynamics problem having nine dynamic state elements and three multiple roots at a specific parameter set. Four different combinations of the two computational acceleration techniques are arranged as in Table 2.

The Ada system at the Texas A&M University supercomputing center utilizes Intel Xeon 2.5 GHz, E5-2670V2 processors and is employed as the computation platform. The programming language for the shooting method solver is MATLAB® 2015 a. Two different multiple core sets, six cores and 12 cores, are applied to the problem for investigating efficiency of the parallel computing. The numbers of generated initial guess for the shooting method are 40, 80, and 120, and the solution procedures are repeated five times to obtain averaged execution times. As can be seen in Fig. 5 and Table 3, the application of the both techniques accelerates the required computations five to eight times faster than the conventional shooting with six cores of central processing unit (CPU), and 12 to 15 times faster with 12 cores of CPU.

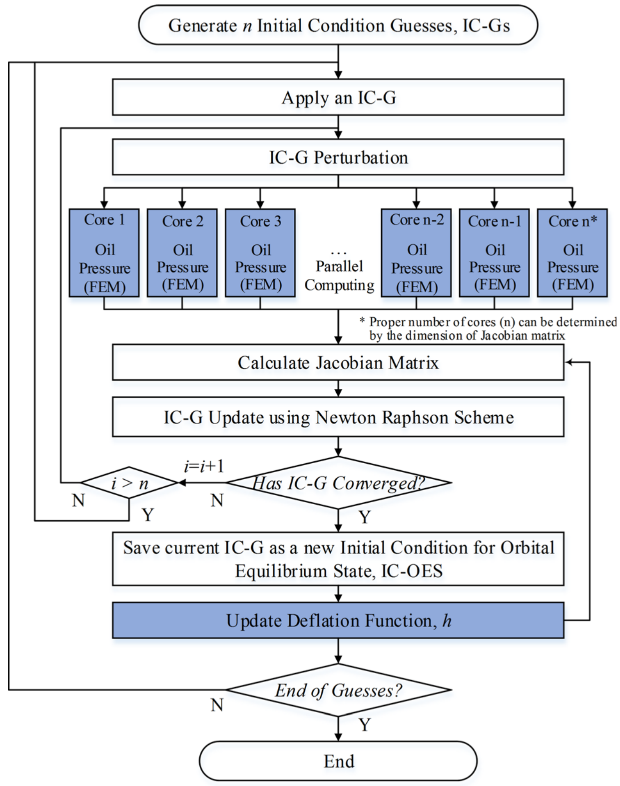

Fig. 4 Flowchart of shooting method with deflation and parallel computing

Table 2 Application sets of the numerical acceleration techniques

	Set #1	Set #2	Set #3	Set #4
Deflation	Not applied	Applied	Not applied	Applied
Parallel computing	Not applied	Not applied	Applied	Applied

3.3 Lyapunov Exponents. Some parameter values result in successive bifurcations progressing to chaos. Various techniques are used in the literature to identify the presence of chaos by implicit and explicit approaches. Lyapunov exponents provide a quantitative indicator by obtaining averaged rates of divergence or convergence of two infinitesimally close trajectories onto an attractor in state space. The neighboring solutions exhibit exponential growth or exponential decay (i.e., $d(t)\sim d_0e^{\lambda t}$). Since n independent initial vectors in n-dimensional space are tested to calculate the rate of the separation, there is a spectrum of Lyapunov exponents λ_i $(i=1, 2,\ldots, n)$. The maximum value of the Lyapunov spectrum $\lambda_{\max}$ can be a critical indicator to determine stability of local responses

- $\lambda_{\max}<0$: system attracts to a fixed point or stable limit cycle (asymptotic stability).
- $\lambda_{\max}=0$: system is neutrally stable (Lyapunov stability).
- $\lambda_{\max}>0$: system is chaotic and unstable.

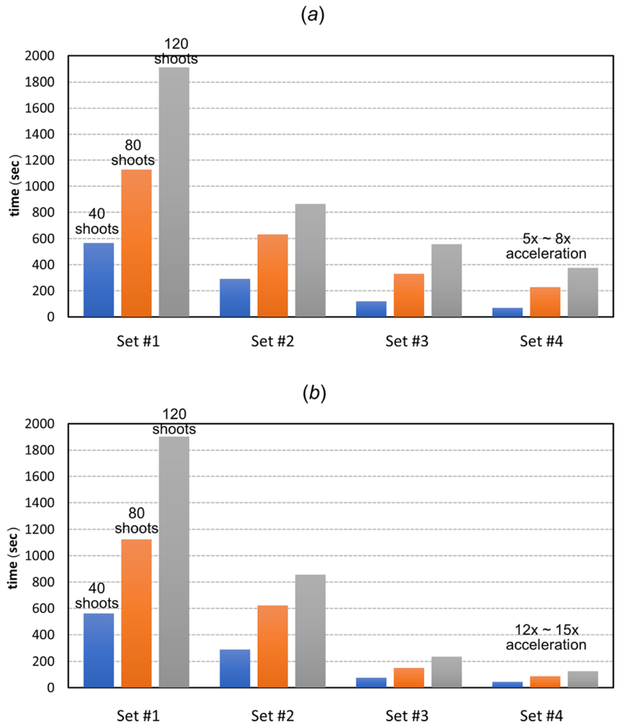

Fig. 5 Computation time of shooting method for solving a three-multiple root nonlinear equation problem with the computation acceleration techniques. (*a*) Computation time with 6 cores and (*b*) computation time with 12 cores.

Table 3 Computation time with the numerical acceleration techniques

Six cores	Set #1	Set #2	Set #3	Set #4
40 shoots	564 s	288 s	117 s	69.2 s
80 shoots	1128 s	631 s	330 s	228 s
120 shoots	1911 s	865 s	558 s	376 s
12 cores	Set #1	Set #2	Set #3	Set #4
40 shoots	562 s	288 s	77.2 s	43.6 s
80 shoots	1124 s	622 s	151 s	87.5 s
120 shoots	1902 s	857 s	236 s	126 s

4 Simulation Results and Discussion

In order to investigate bifurcations and nonlinear behaviors of TPJB-RGD system, both the direct NI and shooting/arc-length continuation are applied with various operating conditions.

4.1 Bifurcation Analysis With Direct Numerical Integration. Use of direct NI can provide bifurcation diagrams consisting of consecutive collections of Poincaré dots with regard to an operation control parameter. Although this method provides only an incomplete picture regarding multiple, coexisting responses, and their stability, it is still useful for providing a "brute force" means to view some possible responses and rotordynamic bifurcations. For the transient responses, the dynamic differential equations are integrated using the MATLAB® routine ode15s, for 300 revolution periods, and steady-state is assumed to occur during the last 100 revolutions. The numerical integration is carried out with a relative tolerance of 10^{-7} in the simulation. As can be seen in Fig. 6, a bifurcation diagram, which shows the nondimensional vertical journal motion, y/C_b, at each spin period, is plotted versus rpm. This presentation is conducted for different parameters of imbalance eccentricity and bearing load.

As a result, lightly loaded and low unbalance cases generally show stabilized vibrations such as synchronous response over all the traversed speed range. In contrast, heavily loaded and high unbalance cases exhibit period doubling bifurcations and subsynchronous responses at high-speed ranges; all the subsynchronous responses emerge after the dynamic unbalance force exceeds the static force (i.e., $F_{\text{imb}}/W > 1$), and the simulations are carried out with the assumption of no contact between the rotor and the bearing pads. The cases of Fig. 6(*c*), with $W = 19.6$ kN, have various response types such as synchronous, subsynchronous, and quasi-/aperiodic motions. For this reason, this bearing load is selected to conduct further analyses such that the bifurcation diagrams are made with different imbalance amounts ranging from $0.02C_b$ to $0.4C_b$.

Combining all the bifurcation diagrams with regards to imbalance eccentricity and spin speed yields the *loci of bifurcations* diagram in Fig. 7. In the diagram, it can be seen that the rotor system has only 1τ periodic response under 8 krpm regardless of the amount of imbalance on the rotor. In contrast, various responses are expected at operation speeds above 8 krpm. For instance, if the rotor system has a constant operating speed of 15 krpm, and it accumulates unbalance due to deposits on the rotor, the system may exhibit various responses in the consecutive forms of $1\tau \rightarrow 2\tau \rightarrow 4\tau \rightarrow$ quasi-periodic/aperiodic as the accumulated unbalance force increases.

It should be noted that this result is obtained from the direct NI method so that multiple responses near the bifurcation locus are not considered. This means that the loci of bifurcations in the figure are not the only solution map for this system, but only one of the multiple possible solution maps. On the other hand, bifurcation diagrams from the shooting/arc-length continuation may provide further regions such as coexistent solutions, response stability, and bifurcation scenarios.

4.2 Bifurcation Analysis With Shooting/Continuation

4.2.1 Bifurcations on Run-Up/Run-Down. The shooting/arc-length continuation methods are applied to the TPJB-RGD system in this section. This appears to be the first application of this rigorous nonlinear dynamics technique to a finite length model of a tilting pad journal bearing. A 14-state model is utilized in the shooting approach with four states for the journal x and y motions and ten states for the motions of the pads. The control parameter of the numerical continuation is the rotor revolution speed (*rev*/*min*), and it is incremented for each harmonic solution that is identified by the shooting method.

To illustrate the results, the maximum and minimum values of the nondimensional vertical displacements, y/C_b, of the periodic solutions are plotted in Fig. 8. This type of diagram is suitable for illustrating: (1) the emergence of periodic solutions and the growth of orbital motions and (2) limit cycles or quasi-periodic or aperiodic motions without massive dots or lines, which may cover other coexisting solutions. Here, the imbalance eccentricity of the disk (e_{imb}) is set as $0.3C_b$. This level of imbalance may be considered large, but not extraordinary, for a high-speed machine. Two practical examples are: (a) compressors that intermittently lose blades due to fatigue or ingestion of debris or (b) machines that operate 24/7 for 5 years between scheduled overhauls. The latter case may lead to accumulated deposits on blades that can be shed resulting in asymmetric deposit distributions and resulting large imbalance. This results in large vibration x–y obits of the journal that have been reported by field engineers to have somewhat polygonal shapes. The large vibrations result in large variations of the film thickness $h(\theta)$ in the bearing. By inspection of Eq. (2) for the pressure field and Eq. (1) for the film thickness $h(\theta)$, the forces are very nonlinear functions of the journal motion (X, Y). This nonlinear dependence produces multiple coexisting solutions some of which emerge or disappear with operational parameter

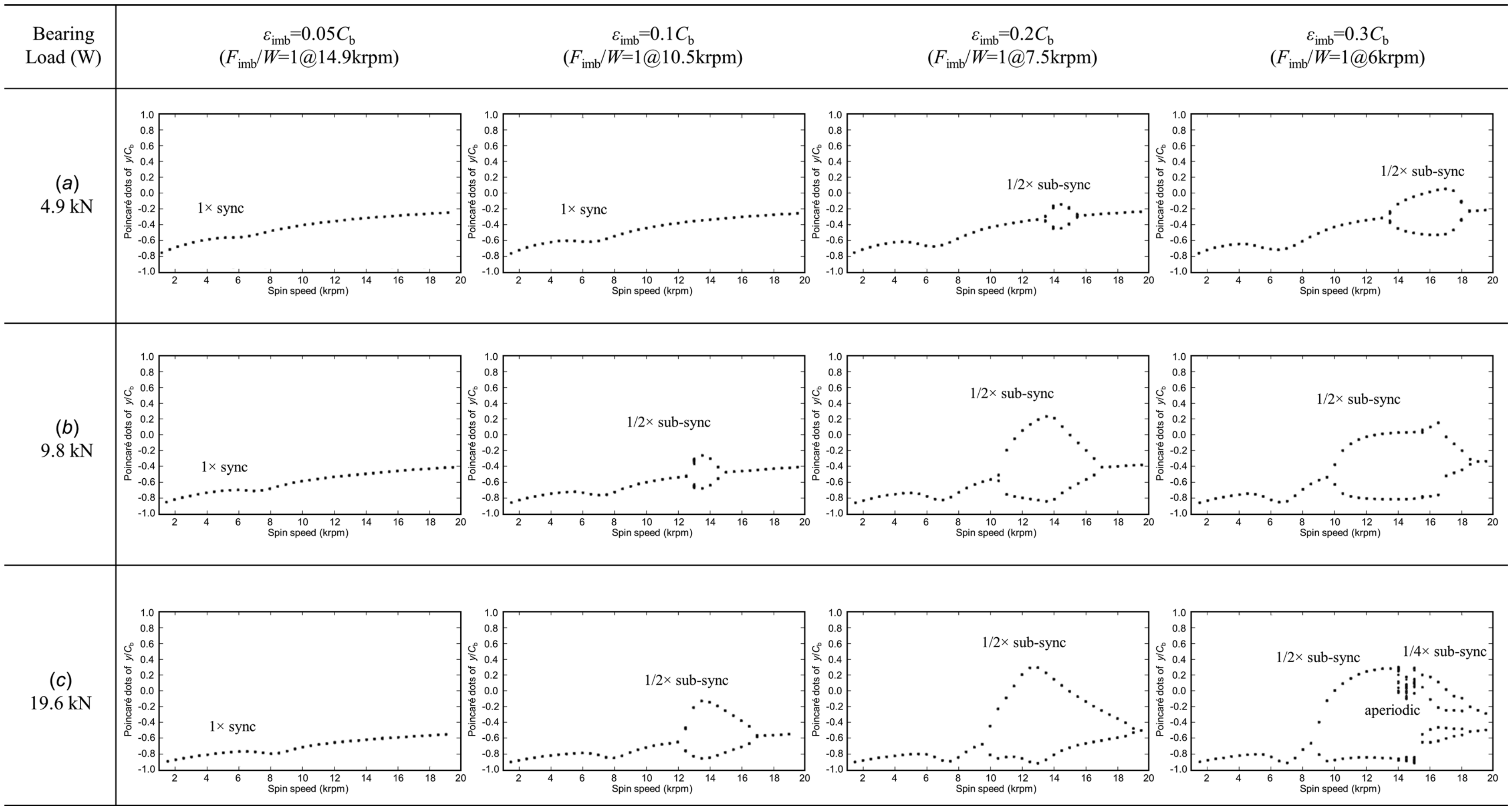

Fig. 6 Bifurcation diagrams with regards to rotor mass and imbalance eccentricity—using direct NI

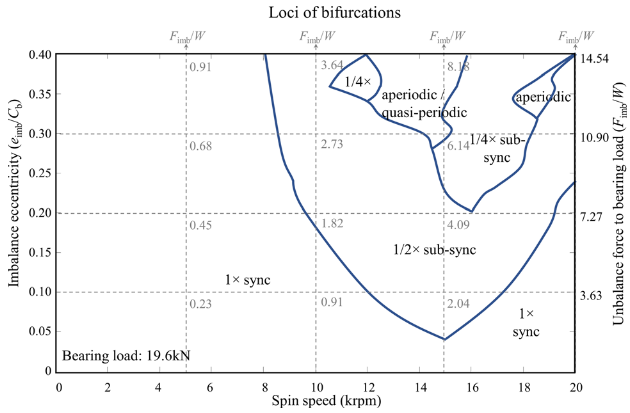

Fig. 7 Loci of bifurcation diagram—using direct NI ($m_p = 1/2$, $\alpha/\beta = 0.5$, and $\mu = 13.8$ mPa·s)

changes, causing bifurcations. As shown in Fig. 8, the small windows connected to the bifurcation diagram show the orbital states of solutions at the specific sections. In case that coexistent solutions are identified, all the solution states are plotted, and the stability of each solution is determined by the Floquet theory.

Over the low spin speed range, the journal maintains a stable $\times 1$ synchronous response and is statically located near the minimum clearance area. A periodic doubling bifurcation occurs at 8.7 krpm, and at the same time the $\times 1$ synchronous response loses its stability and a stable $\times 1/2$ subsynchronous response appears. The orbit of $\times 1/2$ subsynchronous gradually enlarges as rpm increases until 14.1 krpm. Stability of the $^1/_2$ subsynchronous changes to unstable with the appearance of aperiodic motion, but it returns at 14.8 krpm and the aperiodic motion disappears. Then, a stable $\times 1/4$ subsynchronous emerges with the $\times 1/2$ subsynchronous (unstable), and the states last up to 18.2 krpm. Eventually, the two motions converge at 18.2 krpm, and a stable $\times 1/2$ subsynchronous orbit emerges. The unstable $\times 1$ sync persists over the entire speed range above the first bifurcation. From the earlier discussion, it is seen that the numerical continuation approach identifies

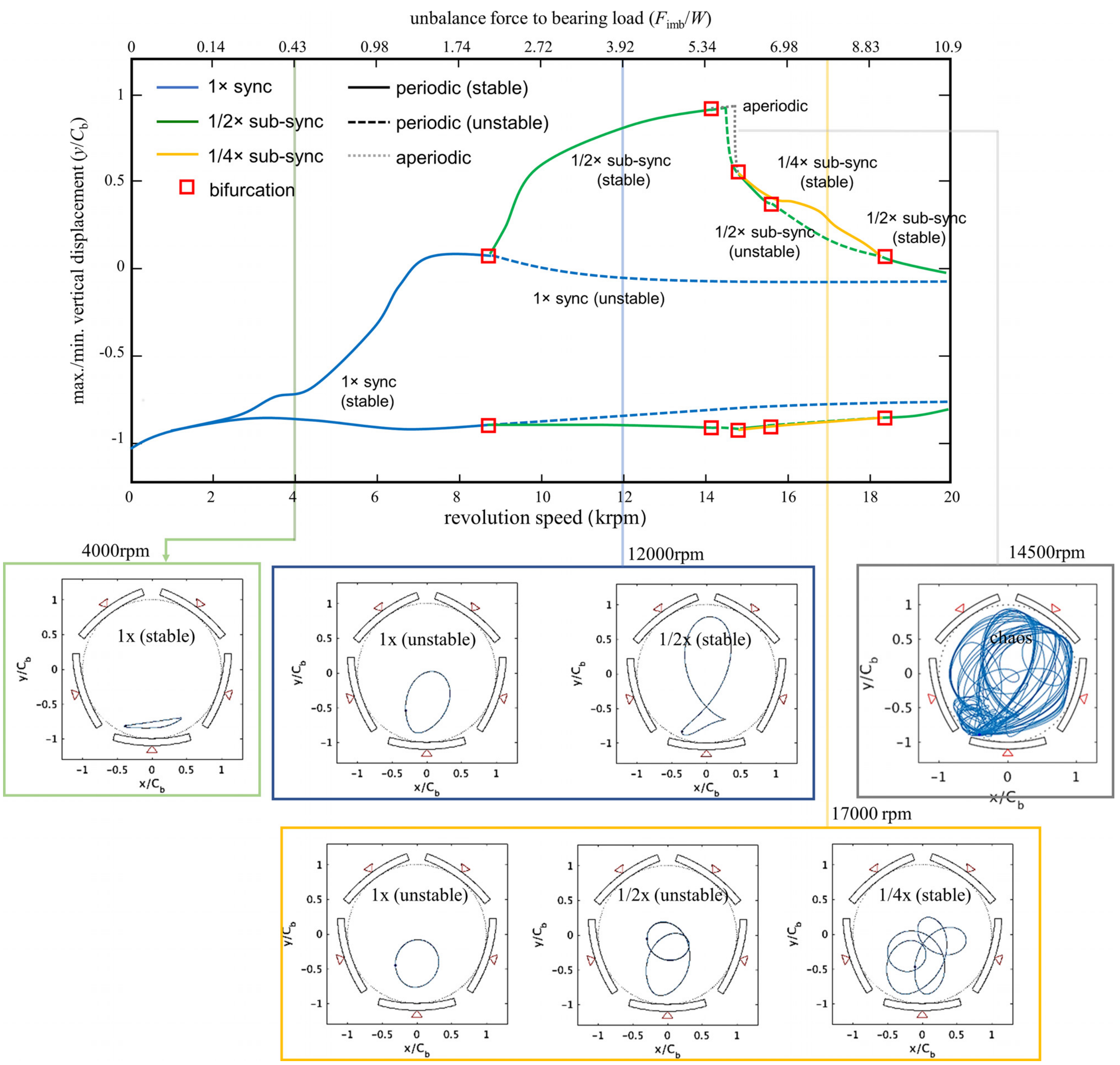

Fig. 8 Bifurcation diagram and coexistent solutions with respect to rotor revolution speed—shooting/continuation ($e_{imb} = 0.3C_b$, $m_p = 1/2$, $\alpha/\beta = 0.5$, and $\mu = 13.8$ mPa·s)

coexisting stable/unstable response states that were previously undetected in the TPJB literature, which relied on numerical integration with arbitrary initial state vectors.

4.2.2 Bifurcations During Accumulating Imbalance on the Rotor. In industrial practice, the balance condition of a rotor system may change over time due to accumulation of deposits on impellers and blades, blade erosion or distortion, shaft bowing, misalignment, etc. These sources produce harmonic forcing of the rotor which as noted in the literature may also affect sub- and superharmonics and bifurcation of vibrations [18,19]. Stopping the operation of a plant in order to balance a machine is always a very costly decision in terms of lost product. On the other hand, failure of a machine due to excessive vibration may lead to an even costlier scenario. Prediction of responses with accumulating unbalance force, during long-term operation, can provide a valuable tool for deciding if a machine should be immediately balanced or repaired.

In order to understand bifurcation scenarios with respect to accumulated imbalance eccentricity, the control parameter of the numerical continuation is set to imbalance eccentricity on the disk with the spin speed fixed at 16 krpm. Figure 9 shows the responses in the low imbalance eccentricity ($e_{\text{imb}} < 0.06C_b$) range maintain a stable $\times 1$ sync state, and then bifurcates into a new $\times 1/2$ subsynchronous response with the stability of the $\times 1$ sync switched to unstable. The orbital motion of $\times 1/2$ subsynchronous gradually enlarges as imbalance increases until $0.21C_b$, which is the onset of a stable $\times 1/4$ subsynchronous. The $\times 1/2$ subsynchronous response has several saddle node bifurcations in the high imbalance condition ($e_{\text{imb}} > 0.27C_b$) so that additional orbital equilibrium states are generated. For example, when the imbalance eccentricity becomes $e_{\text{imb}} = 0.28C_b$, six periodic responses: one

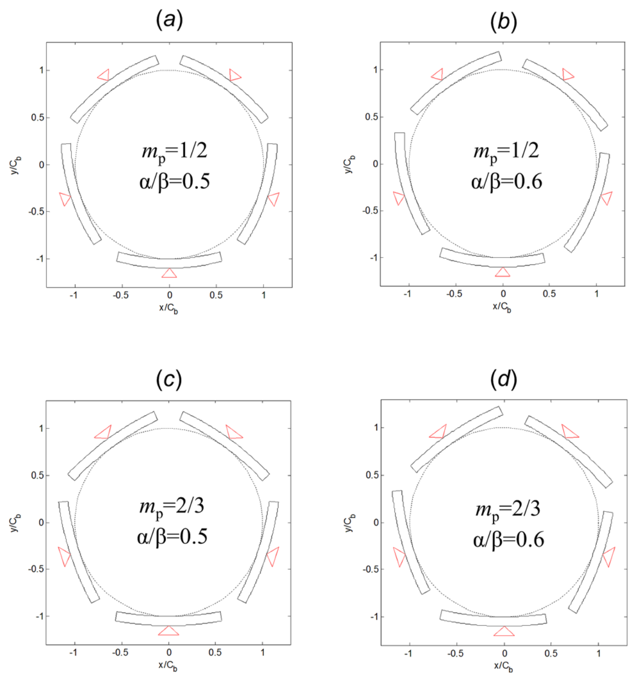

Fig. 10 Geometry of the pad–pivot parameter sets: (*a*) case 1, (*b*) case 2, (*c*) case 3, and (*d*) case 4

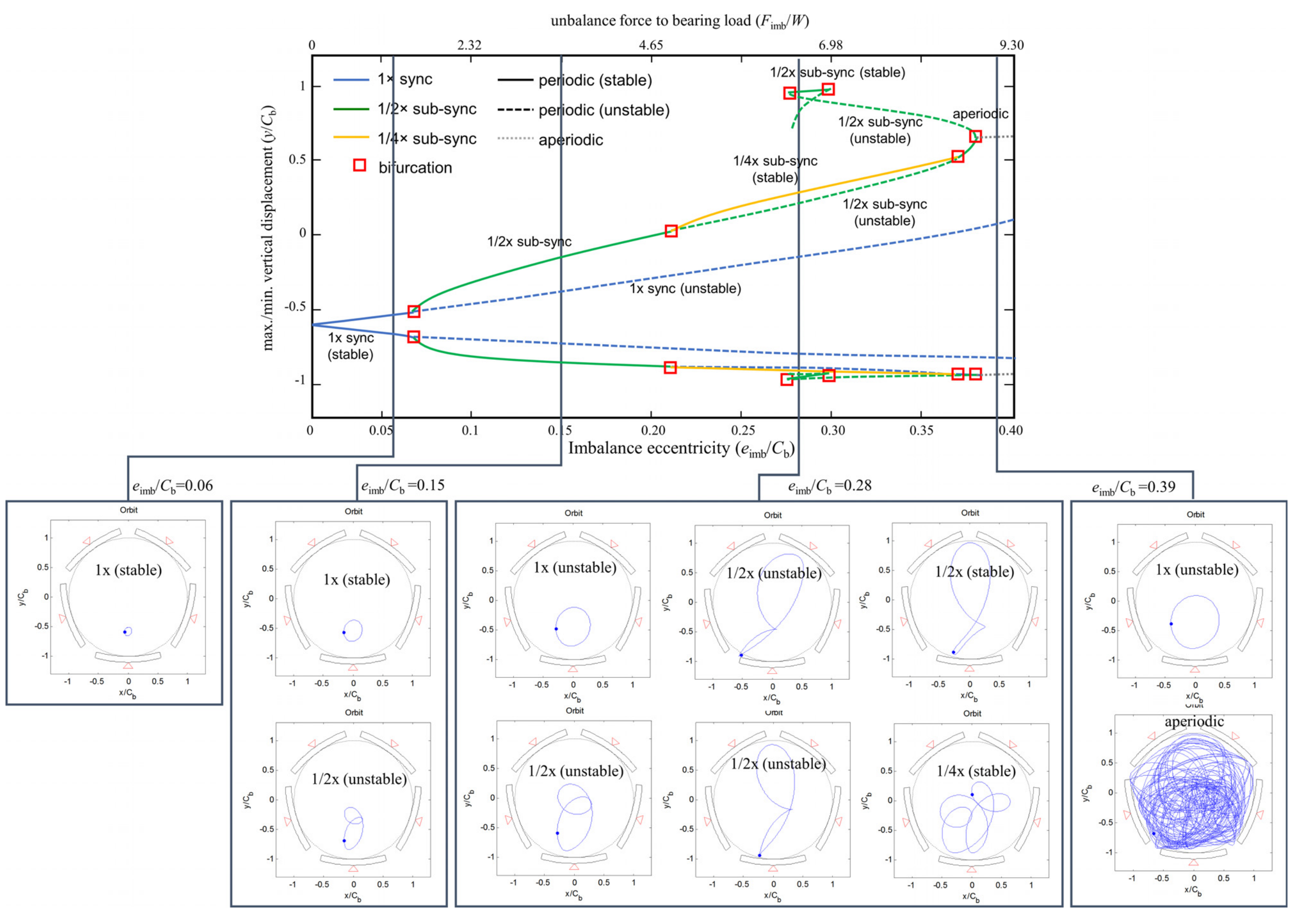

Fig. 9 Bifurcation diagram and coexistent solutions with respect to imbalance eccentricity on disk—shooting/continuation (rpm = 16,000, m_p = 1/2, α/β = 0.5, and μ = 13.8 mPa·s)

×1 sync (unstable), four ×1/2 subsynchronous (stable/unstable), and one ×1/4 subsynchronous (stable) coexist at the identical operating condition. The unstable solutions will not be observed in the time domain response, but may be utilized to aid in identifying the domains of attraction of stable solutions [20]. The subsynchronous responses bifurcate into an aperiodic motion after $0.38C_b$, and the unstable ×1 sync persists throughout the unbalance range, following the first bifurcation.

4.2.3 Effects of Pad Preload and Pivot Offset on Bifurcations. In addition to the current pad preload and pivot offset parameters, i.e., case 1: $m_p = 1/2$, $\alpha/\beta = 0.5$, three pad–pivot geometrical sets: case 2: $m_p = 1/2$, $\alpha/\beta = 0.6$, case 3: $m_p = 2/3$, $\alpha/\beta = 0.5$, and case 4: $m_p = 2/3$, $\alpha/\beta = 0.6$ are chosen for investigating their effects on bifurcations of TPJB-RGD system. Figure 10 depicts the geometry of the respective pad preload and pivot offset cases.

Figure 11 represents the results of the shooting/continuation with the pad–pivot parameter sets. In case 2 ($m_p = 1/2$, $\alpha/\beta = 0.6$) shown in Fig. 11(*a*), it is observed that significant delay of bifurcation onset to the oil whirl (×1/2 subsynchronous), which occurred at $0.07C_b$ with the original set, i.e., case 1, moves to $0.14C_b$. In addition, the emergence of a ×1/4 subsynchronous response that came out of the ×1/2 subsynchronous with periodic doubling bifurcation at $0.21C_b$ disappears over the entire unbalance range. In case 3 ($m_p = 2/3$, $\alpha/\beta = 0.5$) shown in Fig. 11(*b*), it can be seen that the bifurcation onset to oil whirl shifts only by a small amount, i.e., from $0.07C_b$ to $0.085C_b$, so the increased preload over 1/2 seems to have only a minor stabilizing effect. However, the ×1/4 subsynchronous response is observed over an extended range of unbalance, and the high vibration region of ×1/2 subsynchronous, which was located from $0.275C_b$ in the original set, occurs at a lower amount of imbalance eccentricity. Industrial practice typically recommends increasing TPJB preload for increasing rotordynamic stability, defined as the avoidance of all nonharmonic response. This rule of thumb generally holds for small vibrations, however as the present results show is inaccurate for large, nonlinear vibrations. In case 4 ($m_p = 2/3$, $\alpha/\beta = 0.6$) shown in Fig. 11(*c*), the overall bifurcation scenarios are very similar with parameter set 2, but the high vibration states of the ×1/2 subsynchronous response are close to the results from parameter set 3. In that regard, case 4 appears to act qualitatively similar to a combination of sets 2 and 3.

Based on this overview, the pivot location plays a major role in determining the system's response states and bifurcation behavior. The preload has a significant effect on the location and existence of stable, high vibrations of the ×1/2 subsynchronous response near $e_{\text{imb}} = 0.25$–$0.3C_b$.

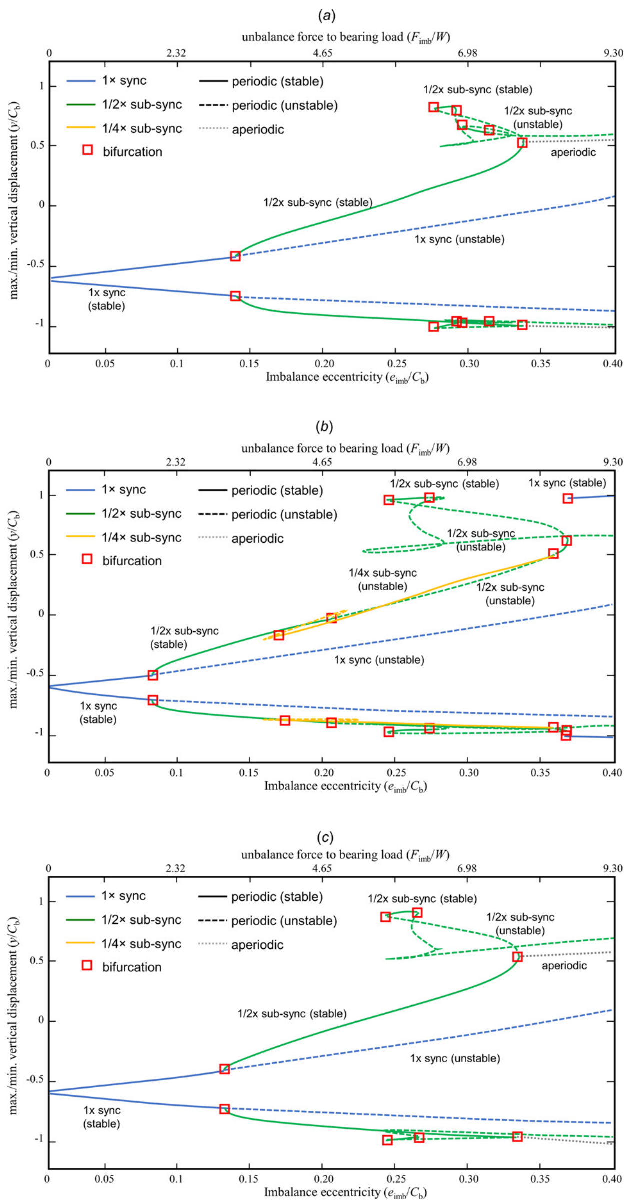

Fig. 11 Bifurcation diagrams with respect to pad preloads (m_p) and pivot offset (α/β): (*a*) case 2 ($m_p = 1/2$ and $\alpha/\beta = 0.6$), (*b*) case 3 ($m_p = 2/3$ and $\alpha/\beta = 0.5$), and (*c*) case 4 ($m_p = 2/3$ and $\alpha/\beta = 0.6$)

4.2.4 Effects of Lubricant Viscosity. In addition to the lubricant viscosity parameter, $\mu = 13.8$ mPa·s, utilized for all previous cases two additional viscosity values $\mu = 27.0$ mPa·s and 10.3 mPa·s, are utilized for investigating the lubricant viscosity effect on the TPJB-RGD system. The oil is assumed to be ISO VG 22, and a corresponding temperature is 45 °C (at $\mu = 27.0$ mPa·s), 65 °C (at $\mu = 13.8$ mPa·s), and 75 °C (at $\mu = 10$ mPa·s),

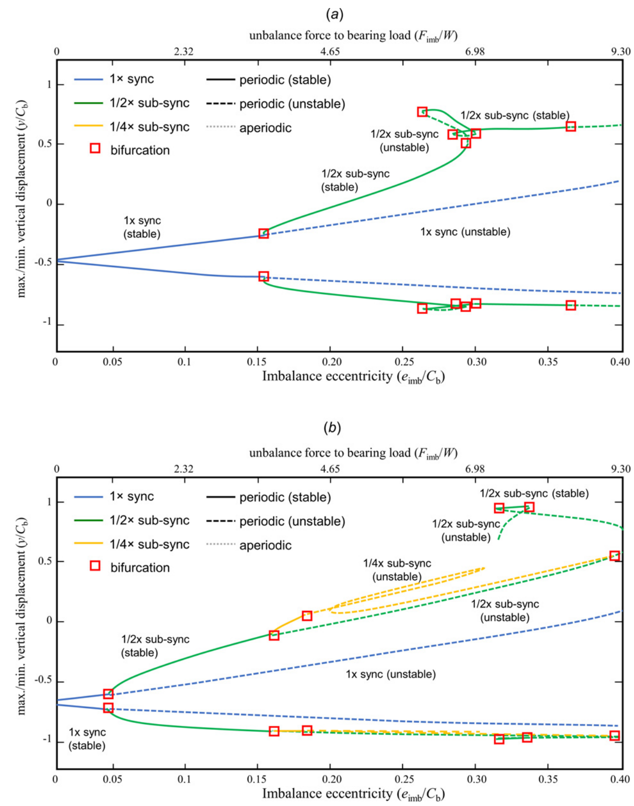

Fig. 12 Bifurcation diagrams ($m_p = 1/2$ and $\alpha/\beta = 0.5$) with lubricant viscosities: (*a*) $\mu = 27.0$ mPa·s and (*b*) $\mu = 10.3$ mPa·s

Table 4 Bifurcation events for lubricant viscosity

Bifurcation events	$\mu = 27.0$ mPa·s	$\mu = 13.8$ mPa·s	$\mu = 10.3$ mPa·s
Onset $\times 1$ sync $\rightarrow \times 1/2$ subsync.	$0.155C_b$	$0.07C_b$	$0.045C_b$
Appearance of $\times 1/4$ subsync.	—(disappeared)	0.21–$0.37C_b$ (net: $0.16C_b$)	0.16–$0.395C_b$ (net: $0.235C_b$)
First saddle node of $\times 1/2$ subsync.	$0.295C_b$	$0.38C_b$	$0.41C_b$

respectively. Figure 12 shows the bifurcation diagrams with the viscosity parameters; here rpm = 16 k.

The result with high viscosity, i.e., $\mu = 27.0$ mPa·s shown in Fig. 12(*a*), shows a more stabilized response behavior over all the unbalance operation range, such that the $1/4$ subsynchronous responses have disappeared, and only $\times 1$ synchronous and $\times 1/2$ subsynchronous remain. In addition, the period doubling bifurcation from $\times 1$ synchronous to $\times 1/2$ subsynchronous is significantly delayed from $0.07C_b$ to $0.155C_b$. The appearance span of the $\times 1/2$ subsynchronous is also reduced. Summarizing, high viscosity delays the onset of $\times 1/2$ subsynchronous and causes the response to transition into quasi-periodic without having any consecutive periodic doubling bifurcations. In contrast, the low viscosity case exhibits a $\times 1/4$ subsynchronous response and extends its appearance span. Similarly, subsynchronous oil whirl emerges at lower rpm than the high viscosity case, and the quasi-periodic motions became dominant in the high imbalance eccentricity range. Low viscosity results in a reduction of film thickness and load capacity, but on a positive note improves (lowers) friction loss. The stability of the $\times 1/4$ subsynchronous turns to unstable after $0.18C_b$, and at the same unbalance level the other periodic solutions, $\times 1$ synchronous and $\times 1/2$ subsynchronous, also become unstable even up to high imbalance eccentricity (although a stable $\times 1/2$ subsynchronous is identified in short range from $0.31C_b$ to $0.33C_b$). This means that a quasi-periodic response dominates above the imbalance amount ($0.18C_b$). Table 4 compares the responses for the three viscosity cases.

4.3 Quasi-Periodic/Aperiodic Motions. As indicated by the above results, the rotor-bearing system response may lose its periodicity, and the response becomes either quasi-periodic or aperiodic. Shooting and arc-length continuation are numerical algorithms for identifying the periodic solutions, so a separate device such as Lyapunov exponents is needed to quantitatively determine the existence of quasi-periodic or chaotic motions. Based on the bifurcation diagram from the direct numerical integrations of the heavily loaded and high unbalance force in Fig. 6(*c*) with $e_{\text{imb}} = 0.3C_b$, the system loses its solution periodicity at high spin speed ranges, which is revealed through the accumulated Poincaré dots on the bifurcation diagram (not shown as single or a few numbers). To examine the character of the aperiodic motions, the maximum Lyapunov exponents (MLEs) are compared with the bifurcation diagram, as can be seen in Fig. 13. Here, steady-state is assumed to occur after 600 revolution periods, after which the MLEs are obtained by means of 600 time intervals with 0.25 revolution per interval. The MLEs are negative values for $\times 1$ synchronous and $\times 1/2$ subsynchronous responses. Figure 13 shows that in certain operating ranges (e.g., 14.5–15.5 krpm and 18.5 krpm), the MLEs exceed or are very close to the chaos boundary, and the values provide further clarification to be interpreted either as quasi- or aperiodic. The Poincaré dots indicate quasi-periodic response at 18 krpm, while the MLEs indicate periodic motion. This inconsistency could result from the limitations of direct numerical integration, which sometimes requires excessive computation time to reach steady-state, especially near an onset of bifurcation. Thus, it can be expected that the response at 18 krpm eventually converges to a periodic solution.

Three samples at 14.5 krpm, 15.5 krpm, and 18.5 krpm are examined in Fig. 14, which displays orbital motions, frequency spectra, and Poincaré maps along with Lyapunov exponent spectra as in Ref. [21]. This approach is very helpful for identifying the

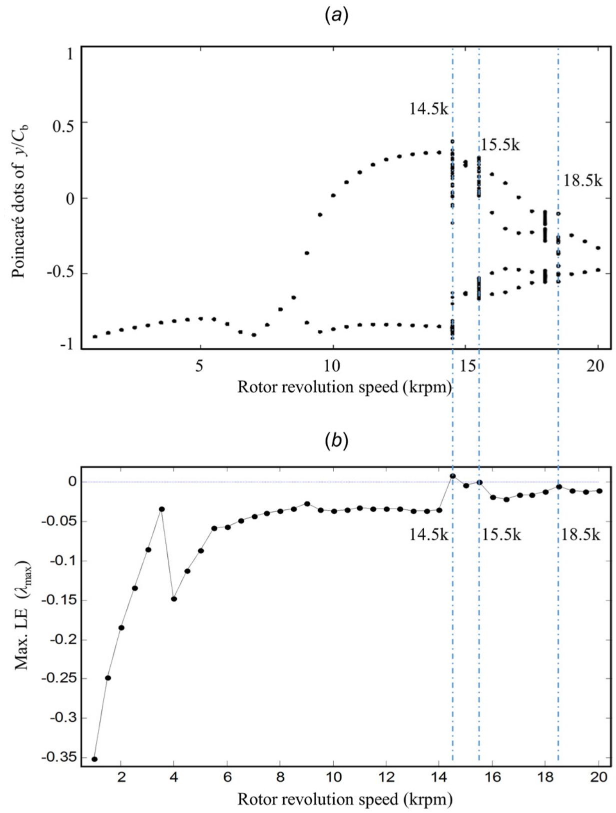

Fig. 13 (*a*) Bifurcation diagram (Poincaré sections) and (*b*) MLE (λ_{max}) plotted versus spin speed ($W = 19.6$ kN, $e_{imb} = 0.3C_b$, $\mu = 13.8$ mPa·s, $m_p = 1/2$, and $\alpha/\beta = 0.5$)

response types. As can be seen in Fig. 14(*a*), which was selected as a chaotic state based on the MLE ($\lambda_{\max} = +0.008$), the orbit is obviously an aperiodic response, the corresponding Poincaré dots form a strange shape, and broadband components are observed in the frequency spectrum. In Fig. 14(*b*), though the MLE is slightly above the critical boundary; $\lambda_{\max} = +0.0008$ and which implies very low chaos. It is assumed that the MLE eventually converges to zero, since the respective orbit and Poincaré represent a quasi-periodic motion. In Fig. 14(*c*), the response which has $\lambda_{\max} = -0.005$ represents periodic motion, and it is also confirmed as an *n*-periodic response by the other response displays.

5 Conclusion

The nonlinear response and bifurcations of a rotor supported by five-pad TPJBs are examined utilizing highly efficient computational algorithms. TPJBs are well known as highly stable when vibration responses are small, but the numerical study shows subsynchronous-, aperiodic-motions, bifurcations, and coexistent solutions can occur under heavily statically loaded and highly dynamically unbalanced conditions. Application of nonautonomous shooting/continuation algorithms implemented with deflation and parallel computing for execution acceleration exhibited various nonlinear behaviors with regards to imbalance eccentricity and spin speed variations. A parametric study with pad geometry

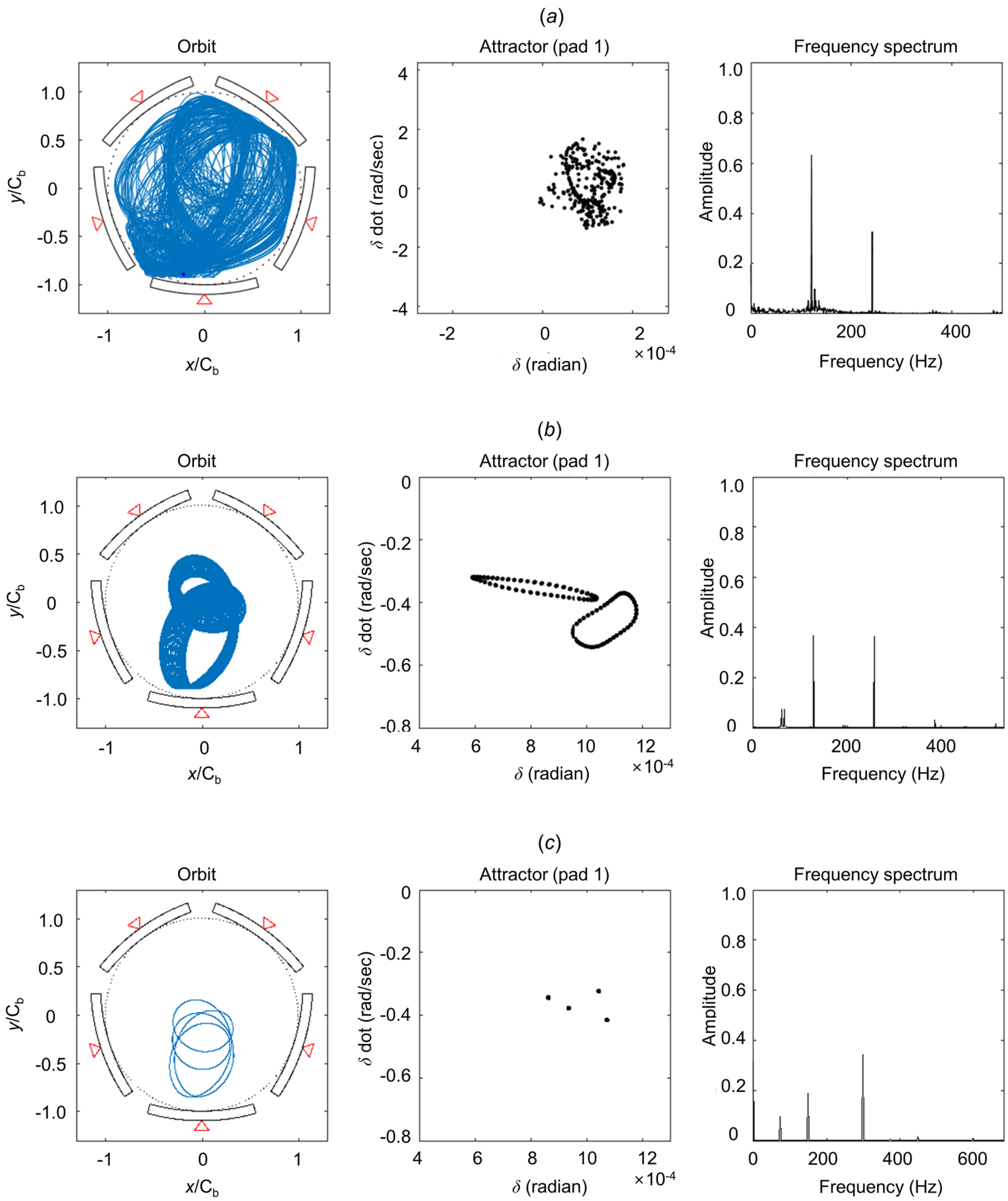

Fig. 14 Orbits, Poincare attractors, and frequency spectra: (*a*) rpm = 14.5 k, (*b*) rpm = 15.5 k, and (*c*) rpm = 18.5 k

confirmed that the pivot location significantly influences nonlinear aspects such that periodic doubling bifurcations and high vibration states are suppressed by locating the pivot point a little after the midplane of the pads (i.e., $\alpha/\beta > 0.5$). On the other hand, the pad preload influences onsets of stable high amplitude $\times 1/2$ subsynchronous responses. Simulations confirmed that lubricant viscosity has a major role on overall response behavior such that higher viscosity tends to suppress the appearance of subsynchronous responses and lower viscosity tends to cause quasi-periodic motion. Lyapunov exponents can explicitly differentiate *n*-periodic-, quasi-periodic, and chaotic responses in TPJBs. Future investigation for bifurcations and nonlinear behaviors in TPJB systems will include a flexible multimass, multidisk rotor model with a modal reduction technique and experimental results.

Acknowledgment

The authors gratefully acknowledge the financial support on this research from the Texas A&M Turbomachinery Research Consortium (TRC).

References

[1] Pagano, S., Rocca, E., Russo, M., and Russo, R., 1995, "Dynamic Behaviour of Tilting-Pad Journal Bearings," Proc. Inst. Mech. Eng., Part J, **209**(4), pp. 275–285.
[2] Brancati, R., Rocca, E., and Russo, R., 1996, "Non-Linear Stability Analysis of a Rigid Rotor on Tilting Pad Journal Bearings," Tribol. Int., **29**(7), pp. 571–578.
[3] Abu-Mahfouz, I., and Adams, M. L., 2005, "Numerical Study of Some Nonlinear Dynamics of a Rotor Supported on a Three-Pad Tilting Pad Journal Bearing (TPJB)," ASME J. Vib. Acoust., **127**(3), pp. 262–272.

[4] Cao, J., Dimond, T. W., and Allaire, P. E., 2013, "Nonlinear Modeling of Tilting-Pad Bearings With Application to a Flexible Rotor Analysis," ASME Paper No. DETC2013-13712.
[5] Gadangi, R. K., and Palazzolo, A. B., 1995, "Transient Analysis of Tilt Pad Journal Bearings Including Effects of Pad Flexibility and Fluid Film Temperature," ASME J. Tribol., **117**(2), pp. 302–307.
[6] Gadangi, R. K., Palazzolo, A. B., and Kim, J., 1996, "Transient Analysis of Plain and Tilt Pad Journal Bearings Including Fluid Film Temperature Effects," ASME J. Tribol., **118**(2), pp. 423–430.
[7] Suh, J., and Palazzolo, A. B., 2014, "Three-Dimensional Thermohydrodynamic Morton Effect Simulation—Part I: Theoretical Model," ASME J. Tribol., **136**(3), p. 031706.
[8] Groll, G., and Ewins, D. J., 2001, "The Harmonic Balance With Arc-Length Continuation in Rotor/Stator Contact Problems," J. Sound Vib., **241**(2), pp. 223–233.
[9] Nataraj, C., and Nelson, H. D., 1989, "Periodic Solutions in Rotor Dynamic Systems With Nonlinear Supports: A General Approach," ASME J. Vib. Acoust. Stress Reliab. Des., **111**(2), pp. 187–193.
[10] Sundararajan, P., and Noah, S. T., 1997, "Dynamics of Forced Nonlinear Systems Using Shooting/Arc-Length Continuation Method—Application to Rotor Systems," ASME J. Vib. Acoust., **119**(1), pp. 9–20.
[11] Sundararajan, P., and Noah, S. T., 1998, "An Algorithm for Response and Stability of Large Order Non-Linear Systems—Application to Rotor Systems," J. Sound Vib., **214**(4), pp. 695–723.
[12] Boyaci, A., Hetzler, H., Seemann, W., Proppe, C., and Wauer, J., 2009, "Analytical Bifurcation Analysis of a Rotor Supported by Floating Ring Bearings," Nonlinear Dyn., **57**(4), pp. 497–507.
[13] Boyaci, A., Seemann, W., and Proppe, C., 2011, "Bifurcation Analysis of a Turbocharger Rotor Supported by Floating Ring Bearings," *IUTAM Symposium on Emerging Trends in Rotor Dynamics*, Springer, Berlin, pp. 335–347.
[14] Amamou, A., and Chouchane, M., 2014, "Nonlinear Stability Analysis of Long Hydrodynamic Journal Bearings Using Numerical Continuation," Mech. Mach. Theory, **72**, pp. 17–24.
[15] Nayfeh, A. H., and Balachandran, B., 2008, *Applied Nonlinear Dynamics: Analytical, Computational and Experimental Methods*, Wiley, New York.
[16] Ojika, T., Watanabe, S., and Mitsui, T., 1983, "Deflation Algorithm for the Multiple Roots of a System of Nonlinear Equations," J. Math. Anal. Appl., **96**(2), pp. 463–479.
[17] Kalantonis, V. S., Perdios, E. A., Perdiou, A. E., Ragos, O., and Vrahatis, M. N., 2003, "Deflation Techniques for the Determination of Periodic Solutions of a Certain Period," Astrophys. Space Sci., **288**(4), pp. 489–497.
[18] Mondy, R. E., 2005, "The Diagnosing and Corrective Actions Taken to Reduce the Effects of Steam Whirl in a General Electric D-11 Steam Turbine," International Symposium for Stability Control of Rotating Machinery (ISCORMA-3), Cleveland, OH, Sept. 19–23, pp. 19–23.
[19] Foiles, W. C., Allaire, P. E., and Gunter, E. J., 1998, "Review: Rotor Balancing," Shock Vib., **5**(5–6), pp. 325–336.
[20] Kim, S., and Palazzolo, A. B., 2016, "Shooting With Deflation Algorithm-Based Nonlinear Response and Neimark-Sacker Bifurcation and Chaos in Floating Ring Bearing Systems," ASME J. Comput. Nonlinear Dyn., **12**(3), p. 031003.
[21] Mongkolcheep, K., Ruimi, A., and Palazzolo, A. B., 2015, "Modal Reduction Technique for Predicting the Onset of Chaotic Behavior Due to Lateral Vibrations in Drillstrings," ASME J. Vib. Acoust., **137**(2), p. 021003.